Lecture 21. Climate Forcing –

Aerosol Direct Radiative Effect

1. CLIMATE FORCING

A. NATURAL FORCING

a. Solar variability

i. Solar sunspots

Most of the radiation emitted by the Sun streams out from its polar regions and from bright rings around the sunspots (dark circular regions). Satellite data have shown a strong correlation between sunspots and solar radiation arriving at Earth, due to a simultaneous mechanism regulating sunspots and solar emission.

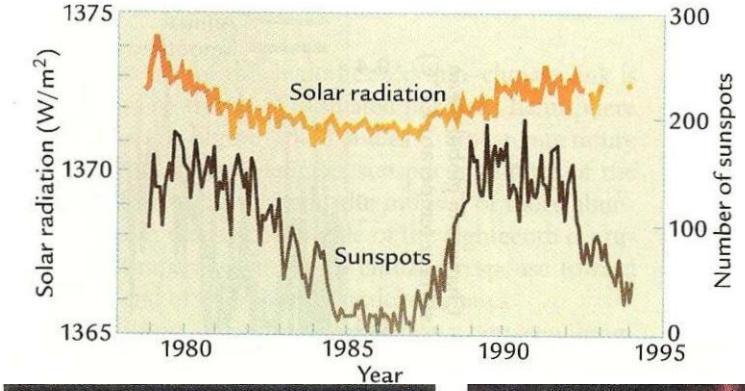

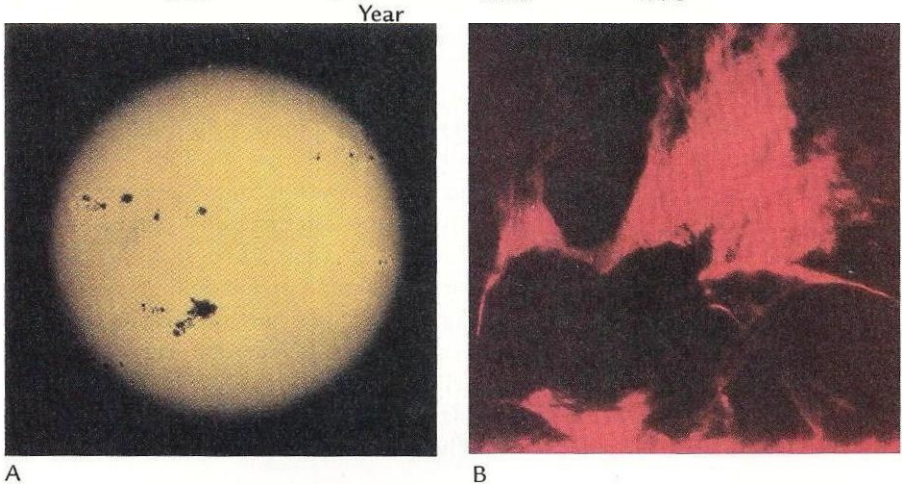

A B

Human observations of cyclic changes in sunspot occurrence through telescopes have been made for almost 500 years. These observations show a regular 11-year sunspot cycle and a minimum during the 17th-century Maunder Minimum.

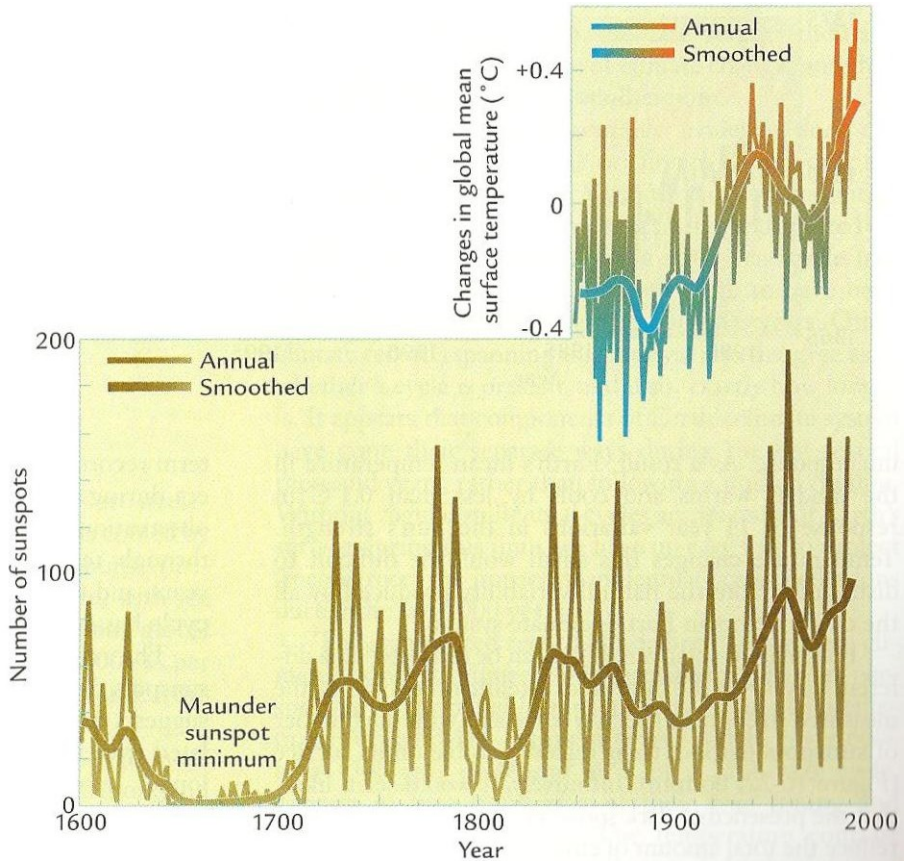

Reconstruction of total solar irradiance at TOA from sunspots varies considerably between studies but all show a present maximum and a Maunder minimum. The difference between the 2 is a net 0.05% increase in total irradiance (0.68 W.m^{-2} in 1,365W.m^{-2}), which corresponds to a RF of 0.12 W.m^{-2} (this IPCC AR4 value is ½ IPCC TAR).

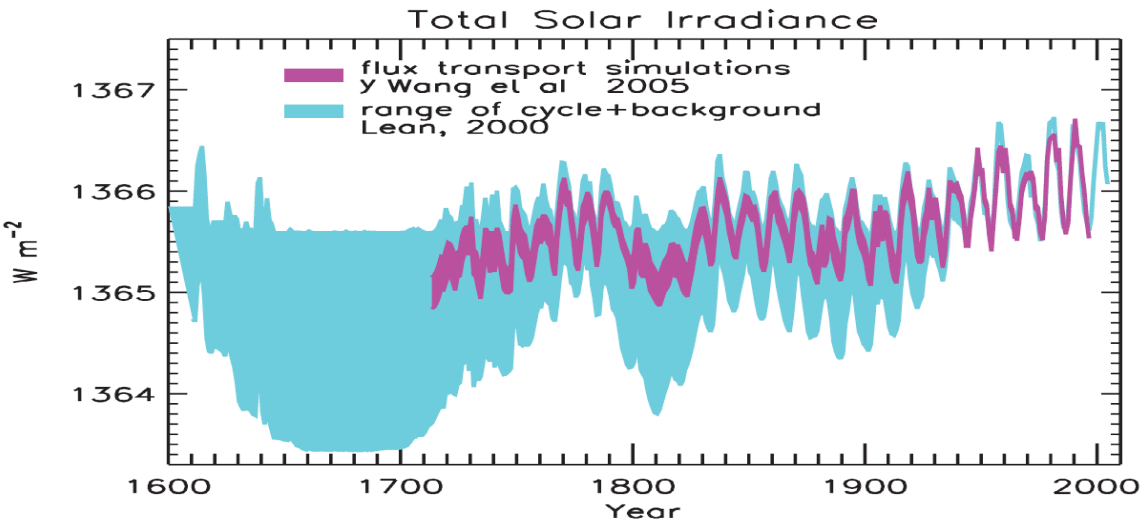

As with solar cycle changes, long-term irradiance variations are expected to have significant spectral dependence. For example, only 1% of Sun's radiant energy is in the UV but is fractionally more variable by at least an order of magnitude.

b. Orbital changes

Periodic changes in characteristics of the Earth's orbit around the Sun control the seasonal and latitudinal distribution of incoming solar radiation (insolation) at the top of the atmosphere.

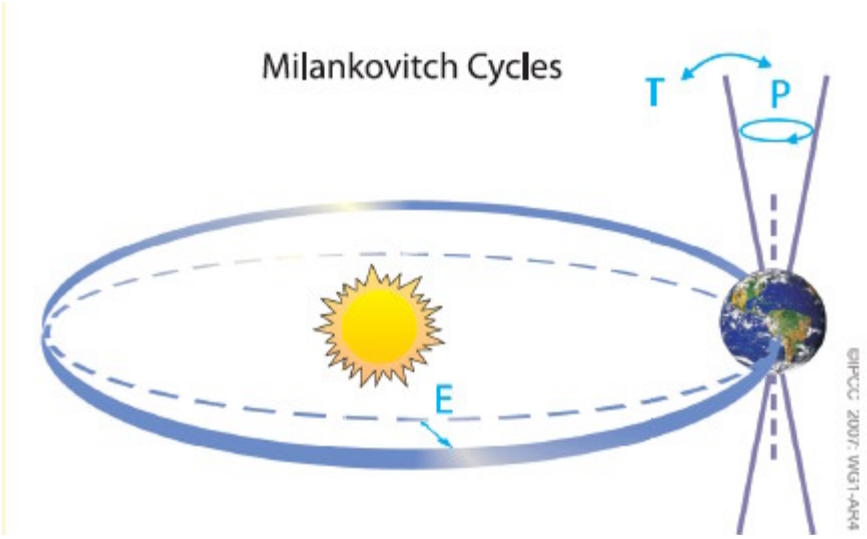

i. Obliquity

The Earth spins around an axis that is tilted from perpendicular to the plane in which the Earth orbits the Sun. This tilt, called obliquity, causes the seasons. At the height of the Northern

Hemisphere winter the North Pole is tilted away from the Sun, while in the summer it is tilted toward the Sun. The angle of the tilt varies between 22° and 24.5° on a cycle of 41,000 years. When the tilt angle is high, the Polar Regions receive less solar radiation than normal in winter and more in summer. The current tilt is 23.3°.

Changes of obliquity modulate seasonal contrast as well as annual mean insolation changes with opposite effects at low vs. high latitude, but there is no effect on global average insolation.

ii. Eccentricity

The eccentricity ε of the elliptical Earth's orbit around the sun is given by $\varepsilon = \frac{\sqrt{a^2 - b^2}}{a}$ where *a* and *b* are half length of the major and minor axis ($a>b$). The eccentricity varies cyclically over time between 0.005 and 0.06. Today value is 0.0167 (close to circular). The periods of major cycles are 100,000 and 413,000 years.

Changes of eccentricity of the Earth's orbit around the Sun have limited impacts on insolation, due to the resulting very small changes in the distance between the Sun and the Earth. However, it may interact with seasonal effects induced by obliquity abd precession of the equinoxes.

iii. Precession

In addition to its daily rotational spin and its yearly revolution around the sun, Earth wobbles slowly like a top, with one full wobble (axial precession) every 25,700 years. Also, the elliptical shape of Earth's orbit rotates with the long and short axes turning slowly in space (procession of the ellipse). The combined procession of the ellipse and axial precession, called the precession of the equinoxes, describe the absolute motion of the equinoxes which has a strong cycle near 23,000 years.

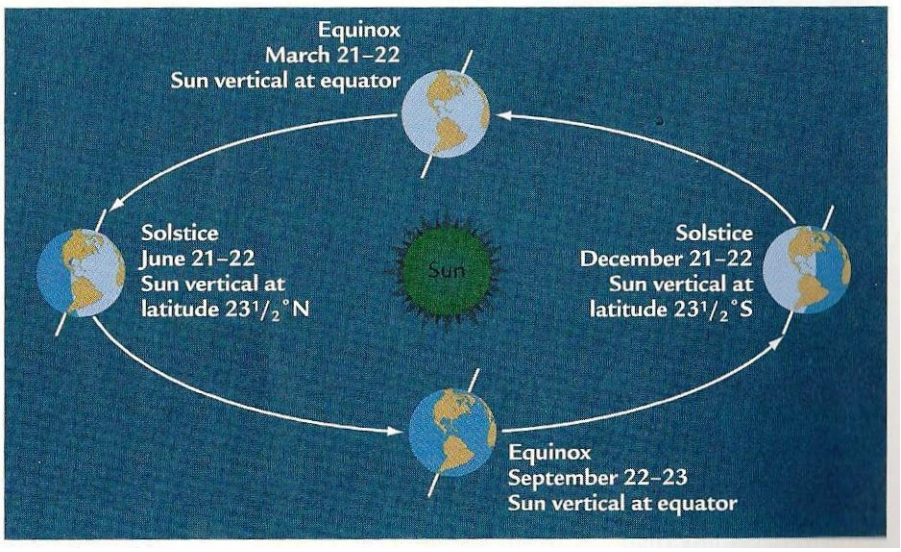

Milankovitch Theory states that cyclic variations of orbital eccentricity, changes in obliquity and precession combine to lead the onset and decline of the major glacial epochs.
Ice ages are generally triggered by minima in high-latitude NH summer insolation, enabling winter snowfall to persist through the year and therefore accumulate to build NH glacial ice sheets. Similarly, times with especially intense high-latitude NH summer insolation, determined by orbital changes, are thought to trigger rapid deglaciations, associated climate change and sea level rise. These orbital forcings determine the pacing of climatic changes, while the large responses appear to be determined by strong feedback processes that amplify the orbital forcing.
Available evidence indicates that the current warming will not be mitigated by a natural cooling trend towards glacial conditions. Understanding of the Earth's response to orbital forcing indicates that the Earth would not naturally enter another ice age for at least 30,000 years. (IPCC AR4 WG1 TS)

c. Volcanic variability

Volcanic eruptions introduce material into the stratosphere (stratospheric volcanic aerosol) that can remain in suspension for one to three years. Volcanic aerosol can reduce solar input by reflecting sunlight back to space, possibly leading to a fall in temperature.

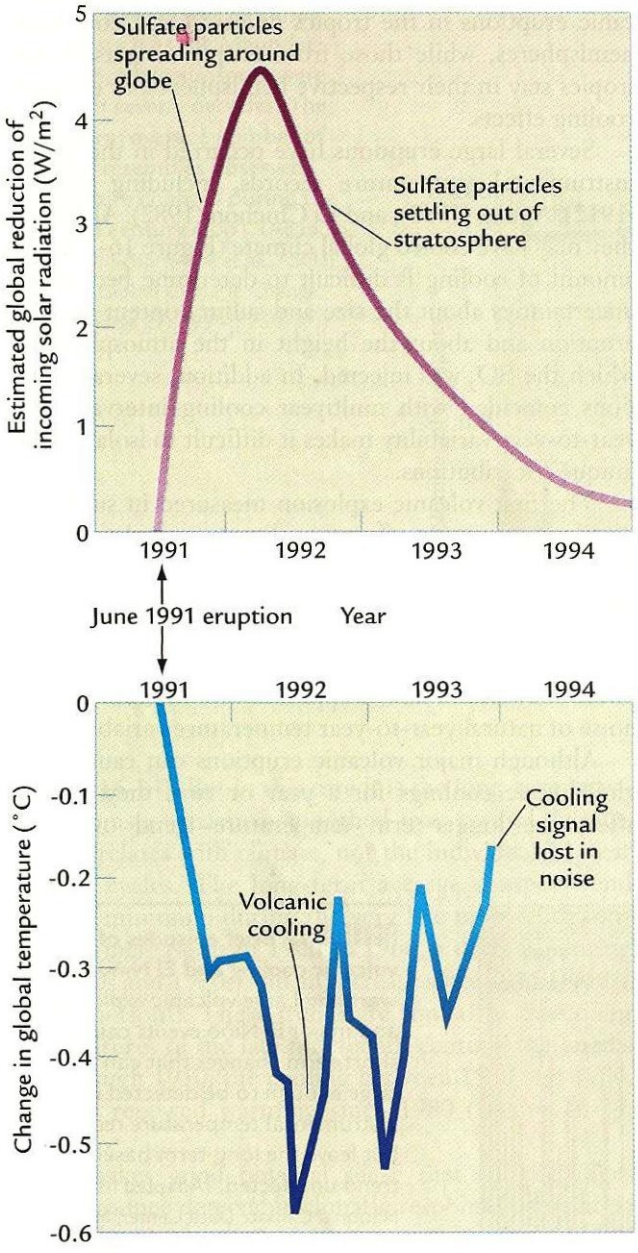
Sulfate particles spreading around globe
Sulfate particles settling out of stratosphere
Estimated global reduction of incoming solar radiation (W/m²)
5
4
3
2
1
0
1991
1992
1993
1994
June 1991 eruption
Year
Cooling signal lost in noise
Volcanic cooling
Change in global temperature (°C)
0
-0.1
-0.2
-0.3
-0.4
-0.5
-0.6

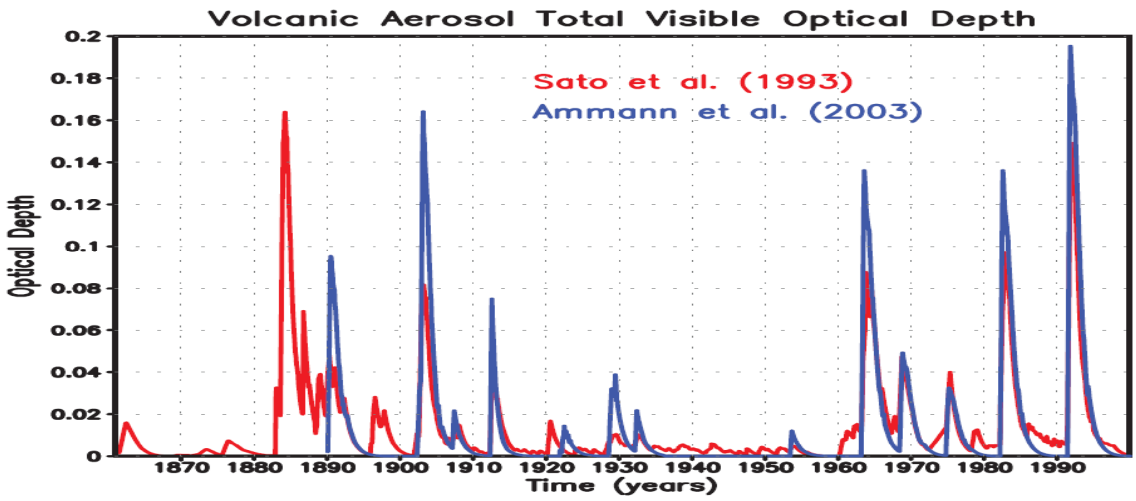

Climate response to Natural Forcing Only

For present climate, *the sum of solar and volcanic forcing would be likely to have produced cooling, not warming. Attribution studies show that it is very likely that these natural forcing factors alone cannot account for the observed warming. There is also increased confidence that natural internal variability cannot account for the observed changes, due in part to improved studies demonstrating that the warming occurred in both oceans and atmosphere.*(IPCC AR4 WG1 TS).

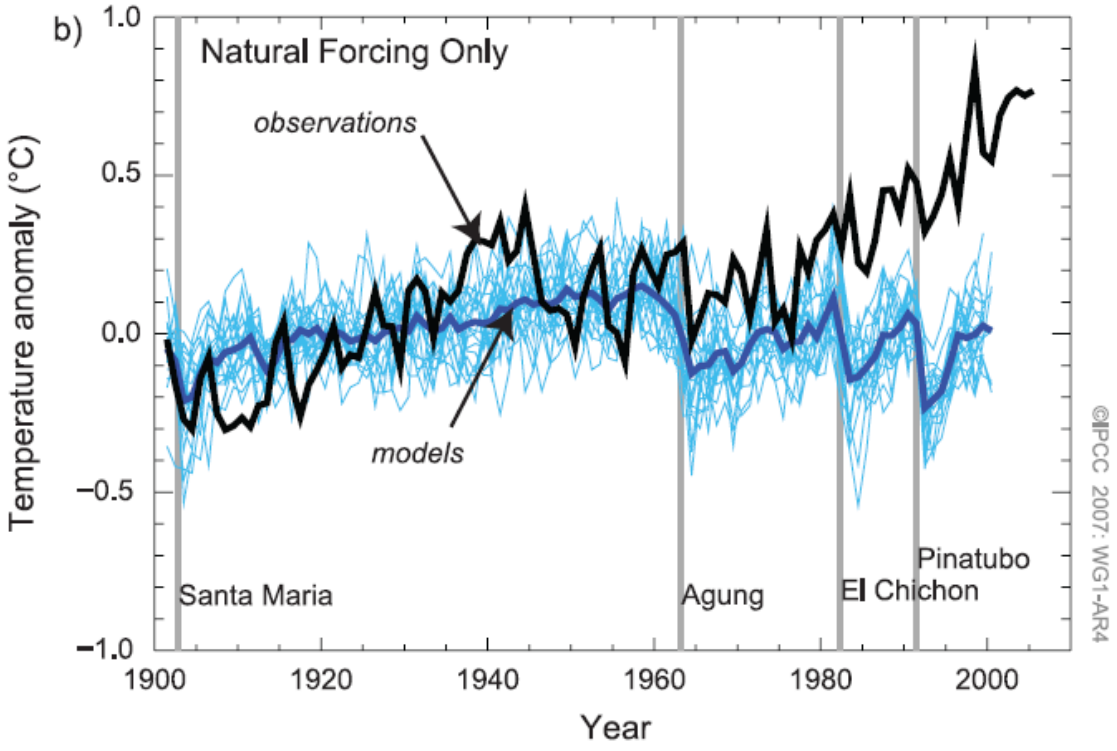

B. ANTHROPOGENIC FORCING

a. **Long-lived Greenhouse Gases (LLGG)**
   i. **Carbon dioxide**

Concentration: 2005: 379 ppm; PI: 275-285ppm
Emission by fossil fuel for transport, industry, domestic use and deforestation
Lifetime: 50-200 years
Monthly concentration and moving average of 5 seasonal cycles

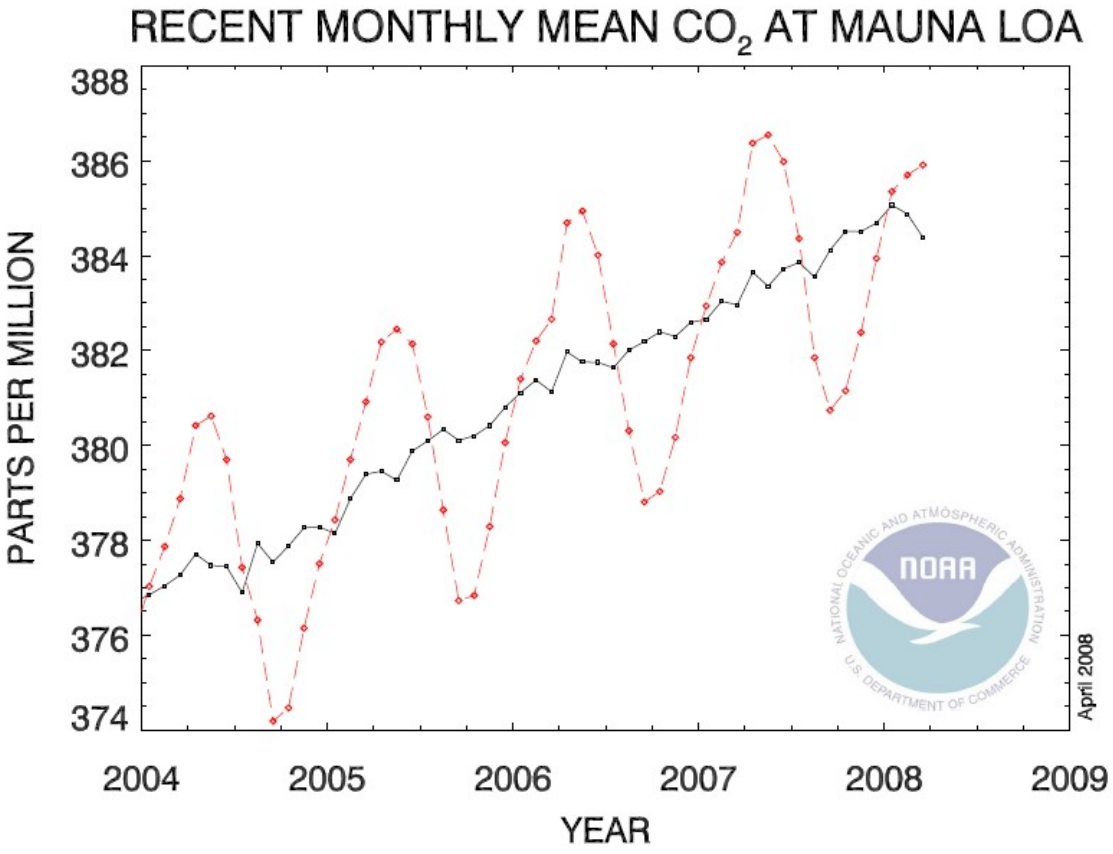

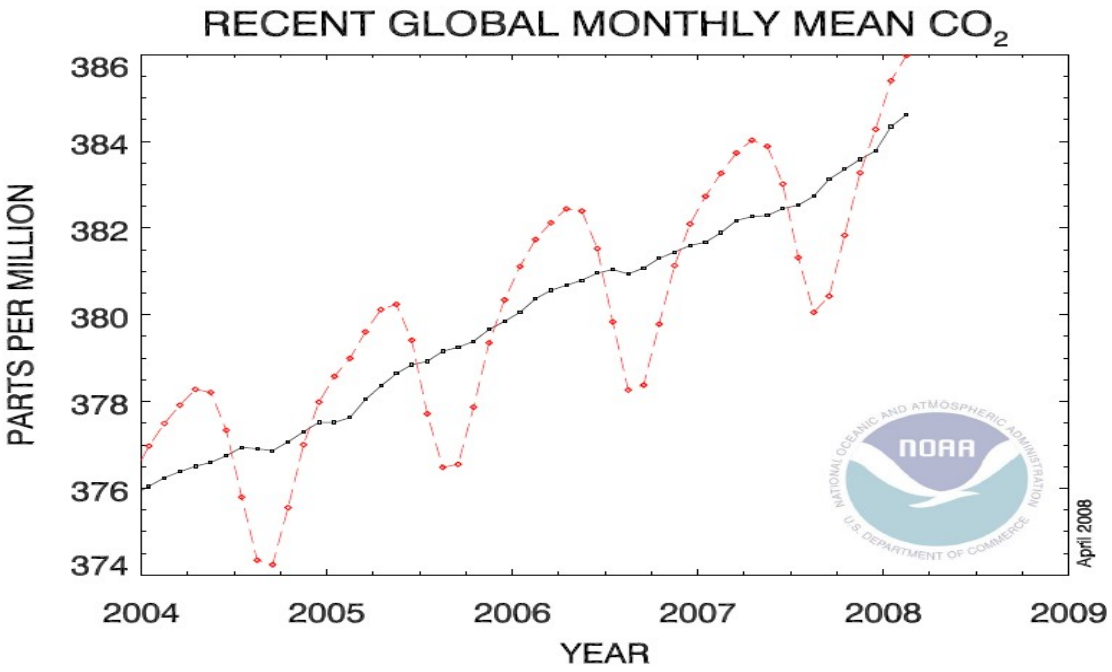

ii. **Methane**

Concentration : 2005 : 1774 ppb; PI: 715 ppb
Emission: Natural (wetlands) + Anthropogenic (agriculture, natural gas distribution, landfills)
Lifetime: Control by OH ~9 years
Reason for reduced growth after 1999: Unknown. Long-term change of OH is negligible, so it may be stabilization in CH4 emission.

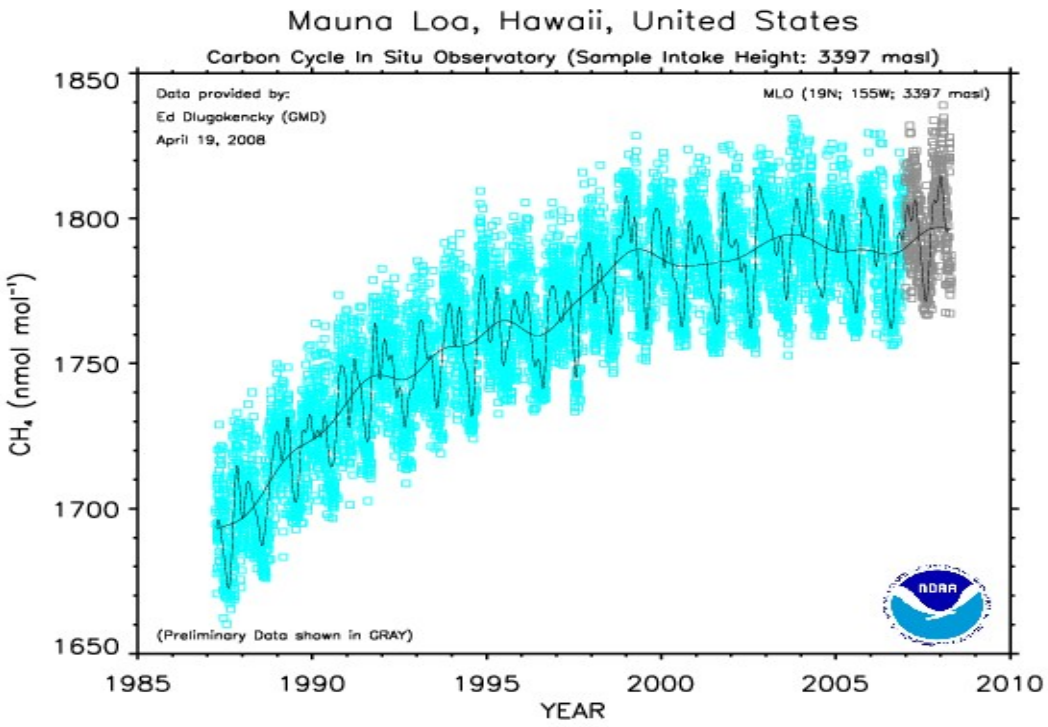

iii. **Nitrous Oxide**

Concentration: 2005: 319 ppb; PI: 270 ppb
Emission: Natural (bacteria in soils+oceans)+Anthro (fertilizer, fossil fuel)

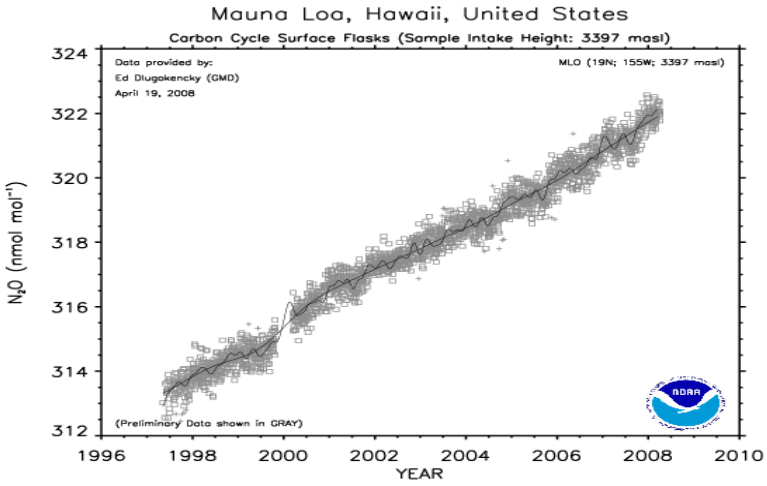

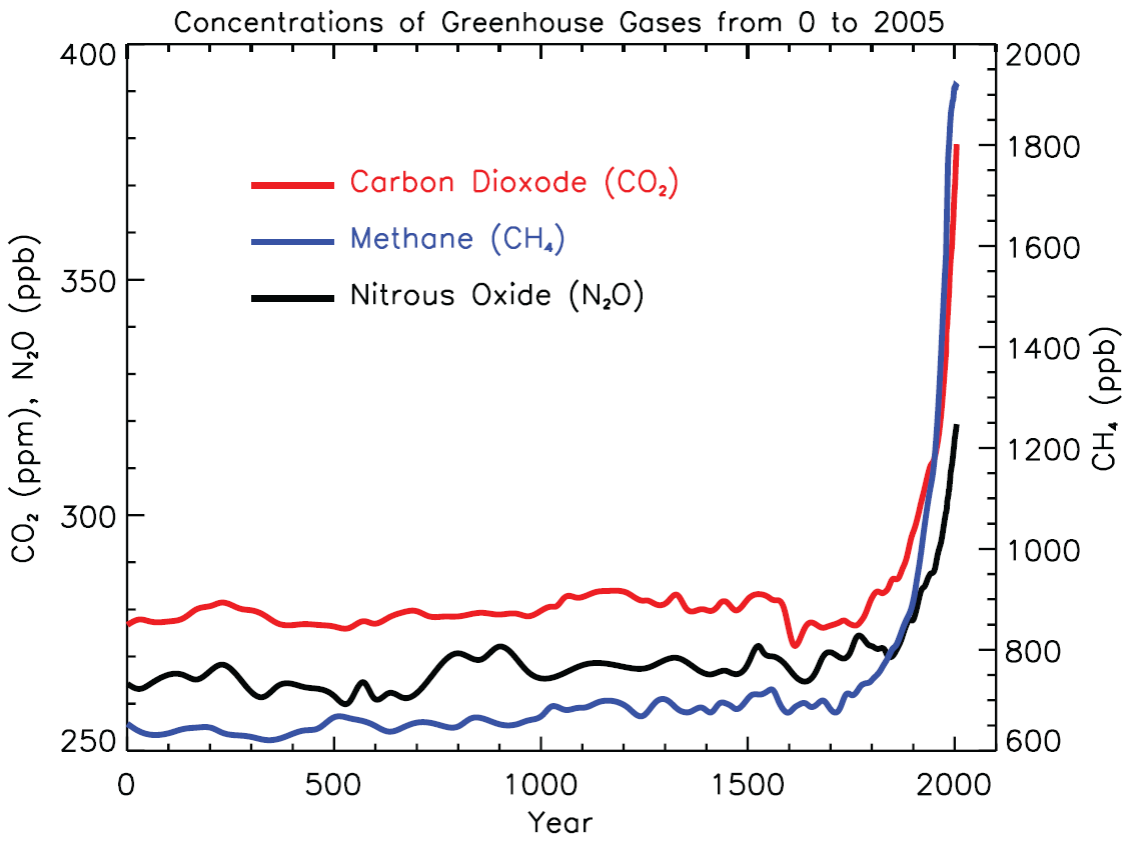

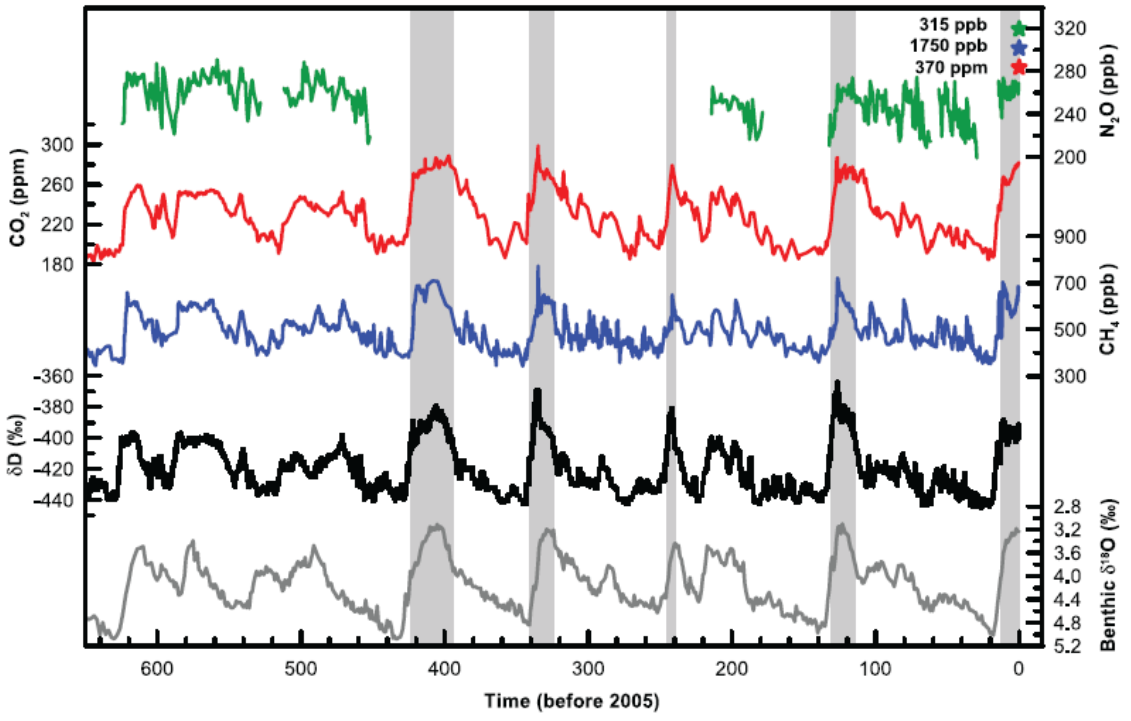

iv. **Halocarbons**

Emission: ~100 tons/year; purely anthropogenic for chlorofluorocarbons (CFC-11, CFC-12); sharp decreases after 1989 due to Montreal protocol (1987)

Lifetime: CFC-11 (55 yr), CFC-12 (140 yr). Photodissociation rates increase by orders of magnitude around 40km high ~10^{-6} s^{-1} (lifetime ~3 months)

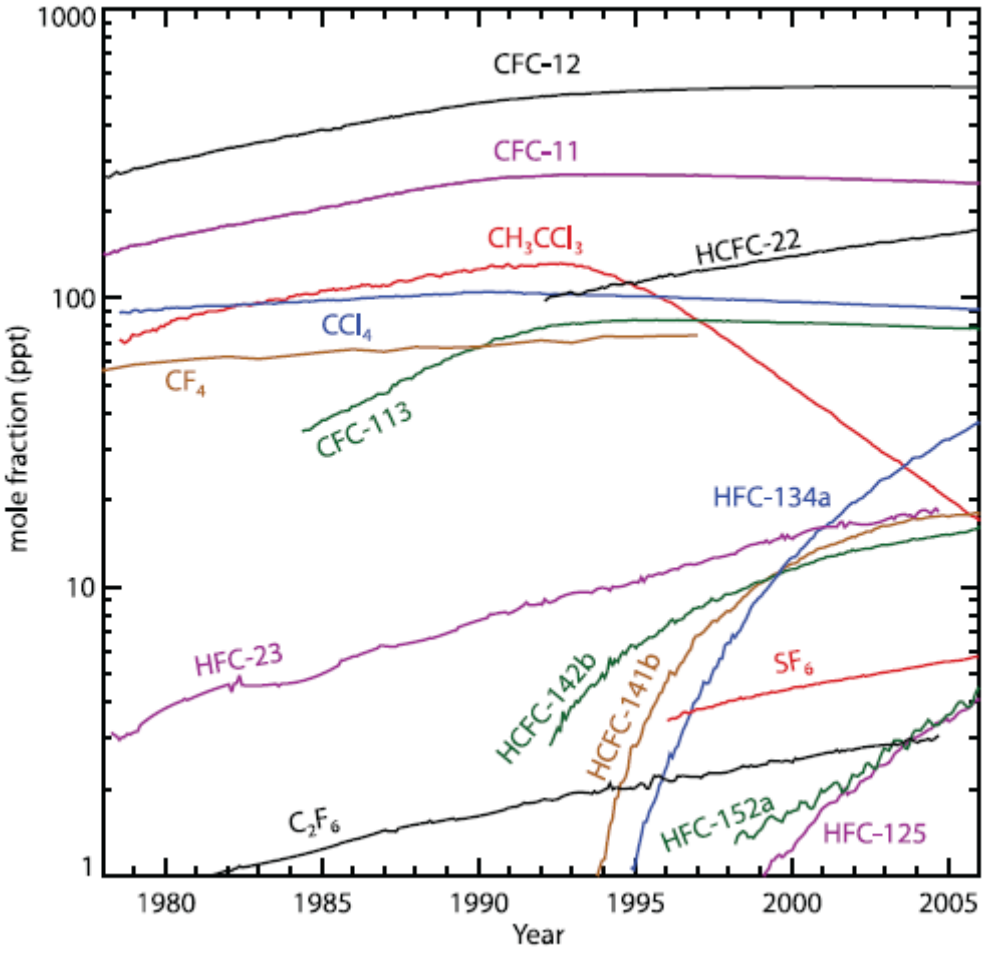

b. **Ozone**

Ozone Column (Strat+Trop) in DU (1 Dobson Unit (DU) is defined to be 0.01 mm thickness at stp) over Uccle (Belgium) from 1972 to 2004: Significant reduction after each major volcanic eruption. After Montreal protocol (1987) O_3 recovery after CFCs reduction.

O3 production from $J(O_2)$ in stratosphere, and from $J(NO_2)+HO_2$ in troposphere. Strongly absorbs in UV. Heterogeneous reaction with sulfate aerosols.

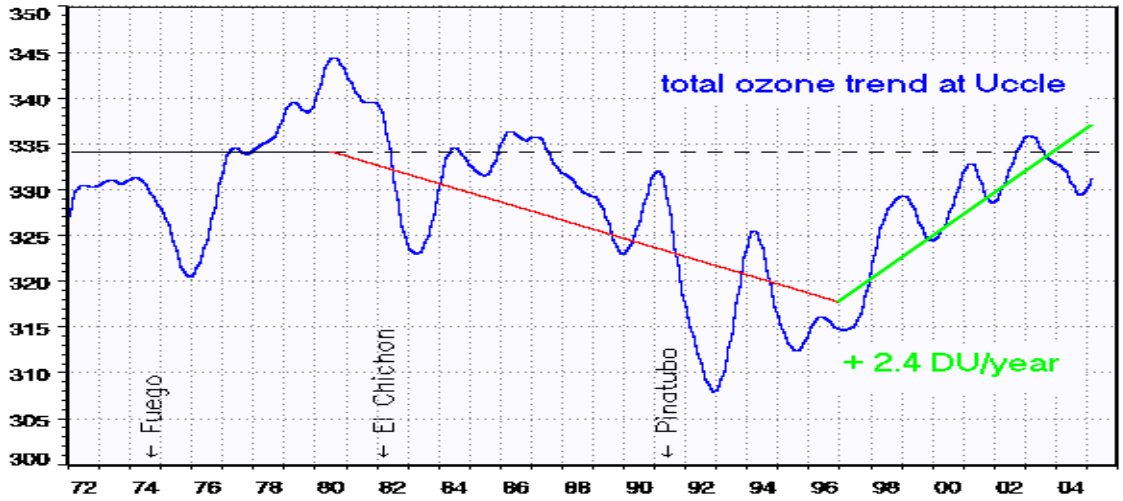

c. Stratospheric Water Vapor

H2O most abundant GHG.
Human weak direct influence on H2O, but significant indirectly by changing climate (warmer climate= more H2O)+ CH4 emissions (CH4+OH->H2O+CH3).

d. Surface Albedo

i. Land use:

Carbon dioxide emissions due to land use changes during the 1990s contributes 6% to 39% of the CO2 growth rate. RF~+0.2 for CO2 release, RF~-0.2 W.m2 for Albedo change

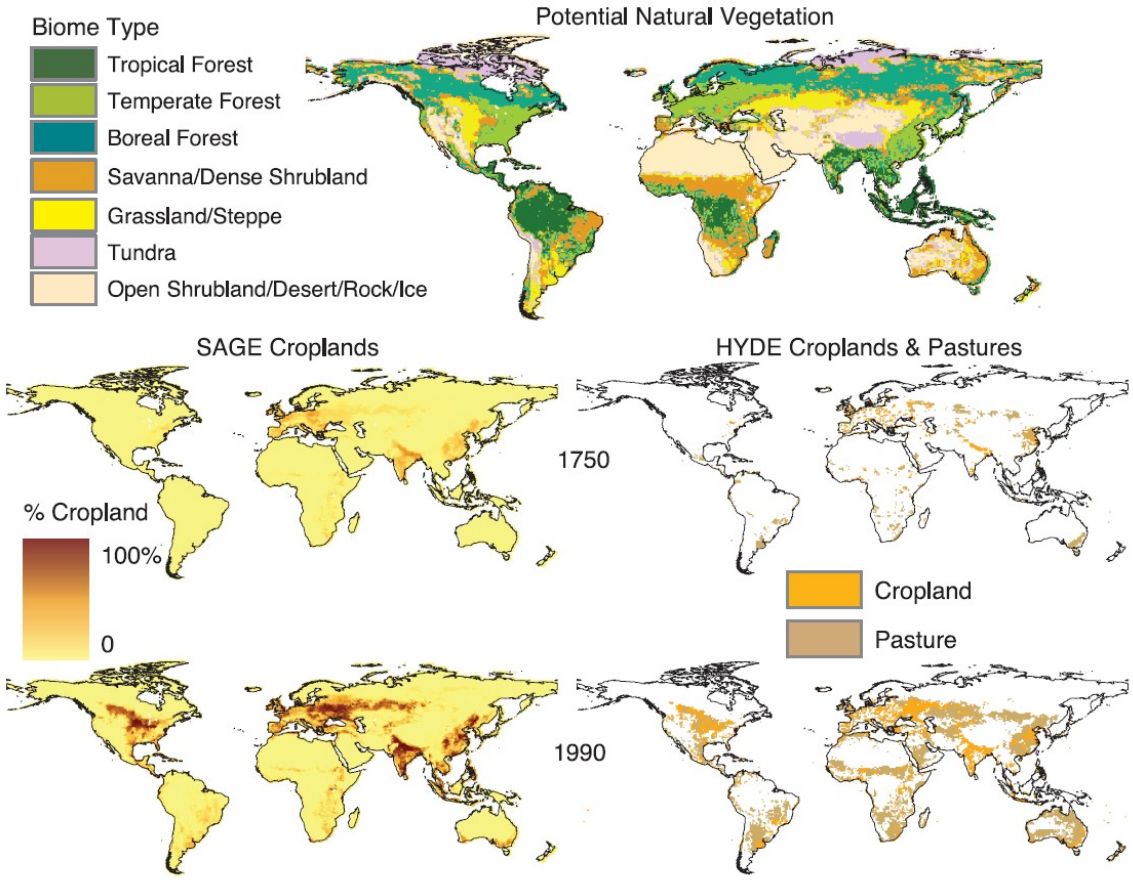

Figure 2.15. *Anthropogenic modifications of land cover up to 1990. Top panel: Reconstructions of potential natural vegetation (Haxeltine and Prentice, 1996). Lower panels: reconstructions of croplands and pasture for 1750 and 1990. Bottom left: fractional cover of croplands from Centre for Sustainability and the Global Environment (SAGE; Ramankutty and Foley, 1999) at 0.5° resolution. Bottom right: reconstructions from the HistorY Database of the Environment (HYDE; Klein Goldewijk, 2001), with one land cover classification per 0.5° grid box.*

ii. Black carbon on snow

Soot on snow => $R_s \Downarrow$ =>RF~+0.15W/m2

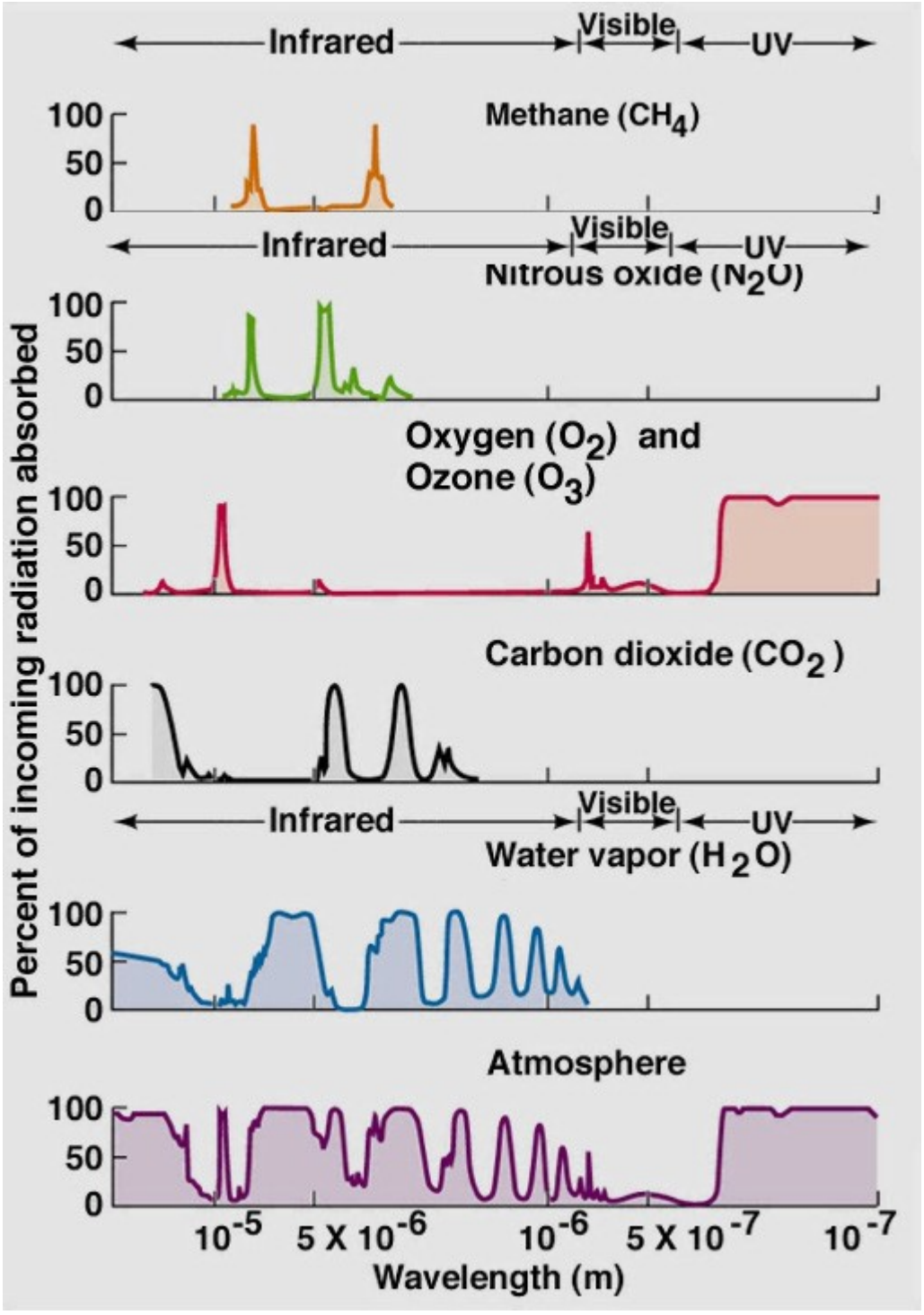
Infrared
Visible
UV
Methane (CH_4)
Nitrous oxide (N_2O)
Oxygen (O_2) and
Ozone (O_3)
Carbon dioxide (CO_2)
Water vapor (H_2O)
Atmosphere
100
50
0
Percent of incoming radiation absorbed
10^{-5}
5 X 10^{-6}
10^{-6}
5 X 10^{-7}
10^{-7}
Wavelength (m)

	Concentrations[b] and their changes[c]		Radiative Forcing[d]	
Species[a]	2005	Change since 1998	2005 ($W m^{-2}$)	Change since 1998 (%)
CO_2	**379 ± 0.65 ppm**	**+13 ppm**	**1.66**	**+13**
CH_4	**1,774 ± 1.8 ppb**	**+11 ppb**	**0.48**	**-**
N_2O	**319 ± 0.12 ppb**	**+5 ppb**	**0.16**	**+11**
	ppt	ppt		
CFC-11	251 ± 0.36	–13	0.063	–5
CFC-12	538 ± 0.18	+4	0.17	+1
CFC-113	79 ± 0.064	–4	0.024	–5
HCFC-22	169 ± 1.0	+38	0.033	+29
HCFC-141b	18 ± 0.068	+9	0.0025	+93
HCFC-142b	15 ± 0.13	+6	0.0031	+57
CH_3CCl_3	19 ± 0.47	–47	0.0011	–72
CCl_4	93 ± 0.17	–7	0.012	–7
HFC-125	3.7 ± 0.10[e]	+2.6[f]	0.0009	+234
HFC-134a	35 ± 0.73	+27	0.0055	+349
HFC-152a	3.9 ± 0.11[e]	+2.4[f]	0.0004	+151
HFC-23	18 ± 0.12[g,h]	+4	0.0033	+29
SF_6	5.6 ± 0.038[i]	+1.5	0.0029	+36
CF_4 (PFC-14)	74 ± 1.6[i]	-	0.0034	-
C_2F_6 (PFC-116)	2.9 ± 0.025[g,h]	+0.5	0.0008	+22
CFCs Total[k]			**0.268**	**–1**
HCFCs Total			**0.039**	**+33**
Montreal Gases			**0.320**	**–1**
Other Kyoto Gases (HFCs + PFCs + SF_6)			**0.017**	**+69**
Halocarbons			**0.337**	**+1**
Total LLGHGs			**2.63**	**+9**

It is *very likely* that anthropogenic greenhouse gas increases caused most of the observed increase in global average temperatures since the mid-20th century. Without the cooling effect of atmospheric aerosols, it is *likely* that greenhouse gases alone would have caused a greater global mean temperature rise than that observed during the last 50 years. A key factor in identifying the aerosol fingerprint, and therefore the amount of cooling counteracting greenhouse warming, is the temperature change through time, as well as the hemispheric warming contrast.

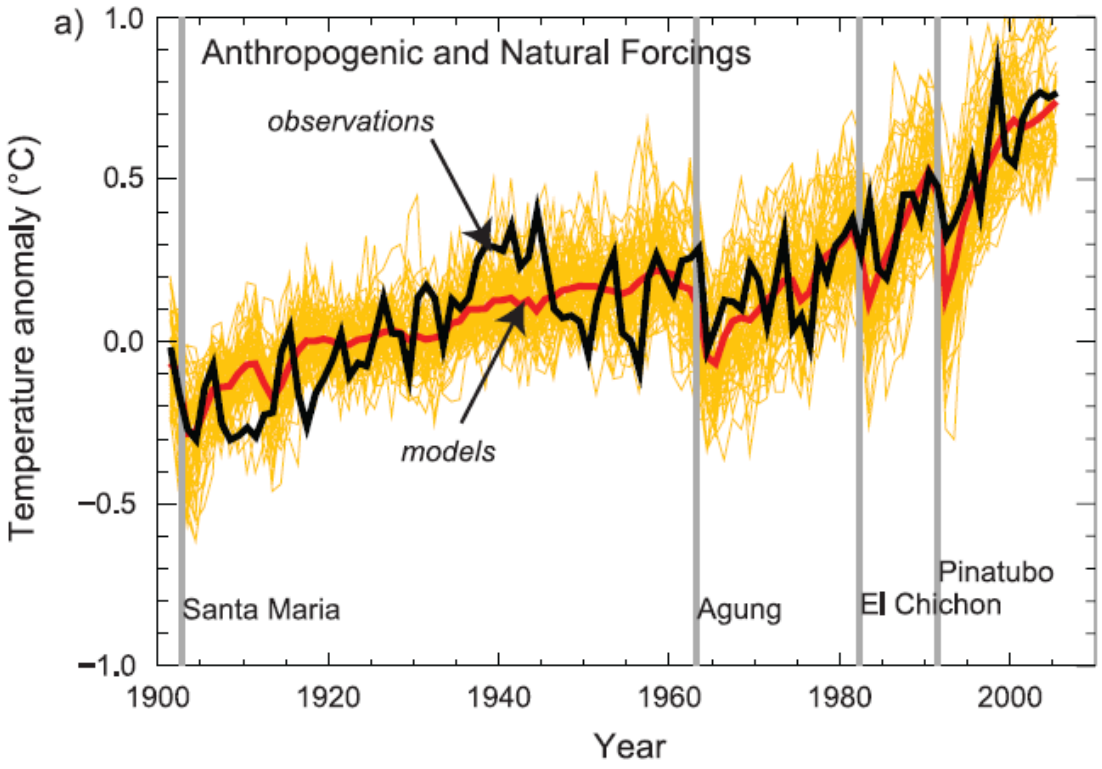
a)
Anthropogenic and Natural Forcings
observations
models
Santa Maria
Agung
El Chichon
Pinatubo
Temperature anomaly (°C)
1.0
0.5
0.0
−0.5
−1.0
1900
1920
1940
1960
1980
2000
Year

2. AEROSOL DIRECT RADIATIVE EFFECT

Direct RF: Aerosols scattering + absorption at SW and LW

Key parameters: ε_e, ω, $P(\theta)$=f(λ, RH)

SW:

- At TOA
  - white aerosols: RF<0
  - brown aerosols:
    - RF<0 over bright surface
    - RF>0 over dark surface
  - Black aerosols: RF>0
- At SFC
  - Whatever the value of RF, reduction of SW irradiance

LW: Significant for large particles at high altitude. Essentially absorption. Important for dust.

- Over land: $T_s >> T_{aer}$ => RF>0
- Over Ocean: $T_s >= T_{aer}$ =>RF>=0

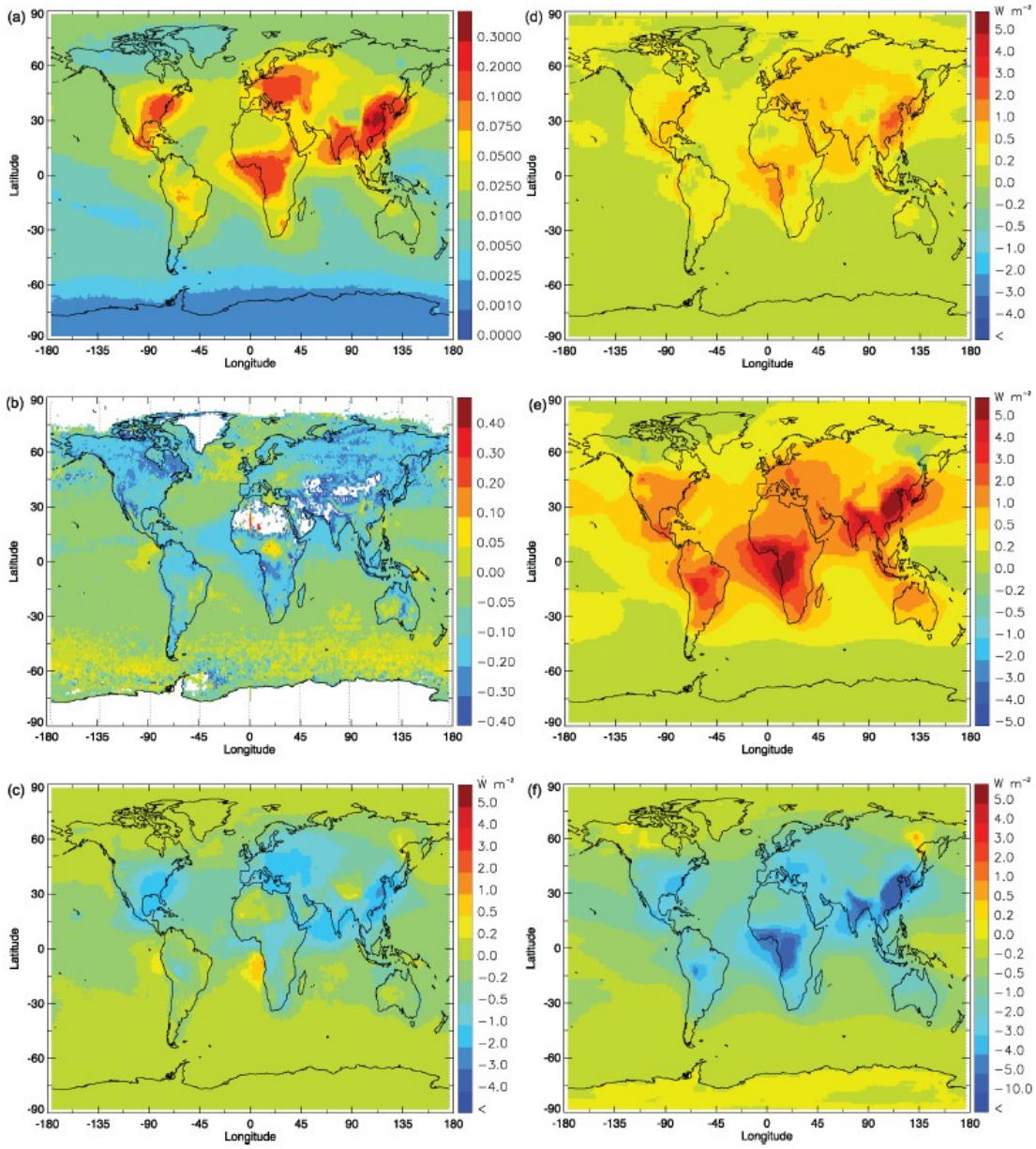

Figure 2.12. *Characteristic aerosol properties related to their radiative effects, derived as the mean of the results from the nine AeroCom models listed in Table 2.5. All panels except (b) relate to the combined anthropogenic aerosol effect. Panel (b) considers the total (natural plus anthropogenic) aerosol optical depth from the models. (a) Aerosol optical depth. (b) Difference in total aerosol optical depth between model and MODIS data. (c) Shortwave RF. (d) Standard deviation of RF from the model results. (e) Shortwave forcing of the atmosphere. (f) Shortwave surface forcing.*

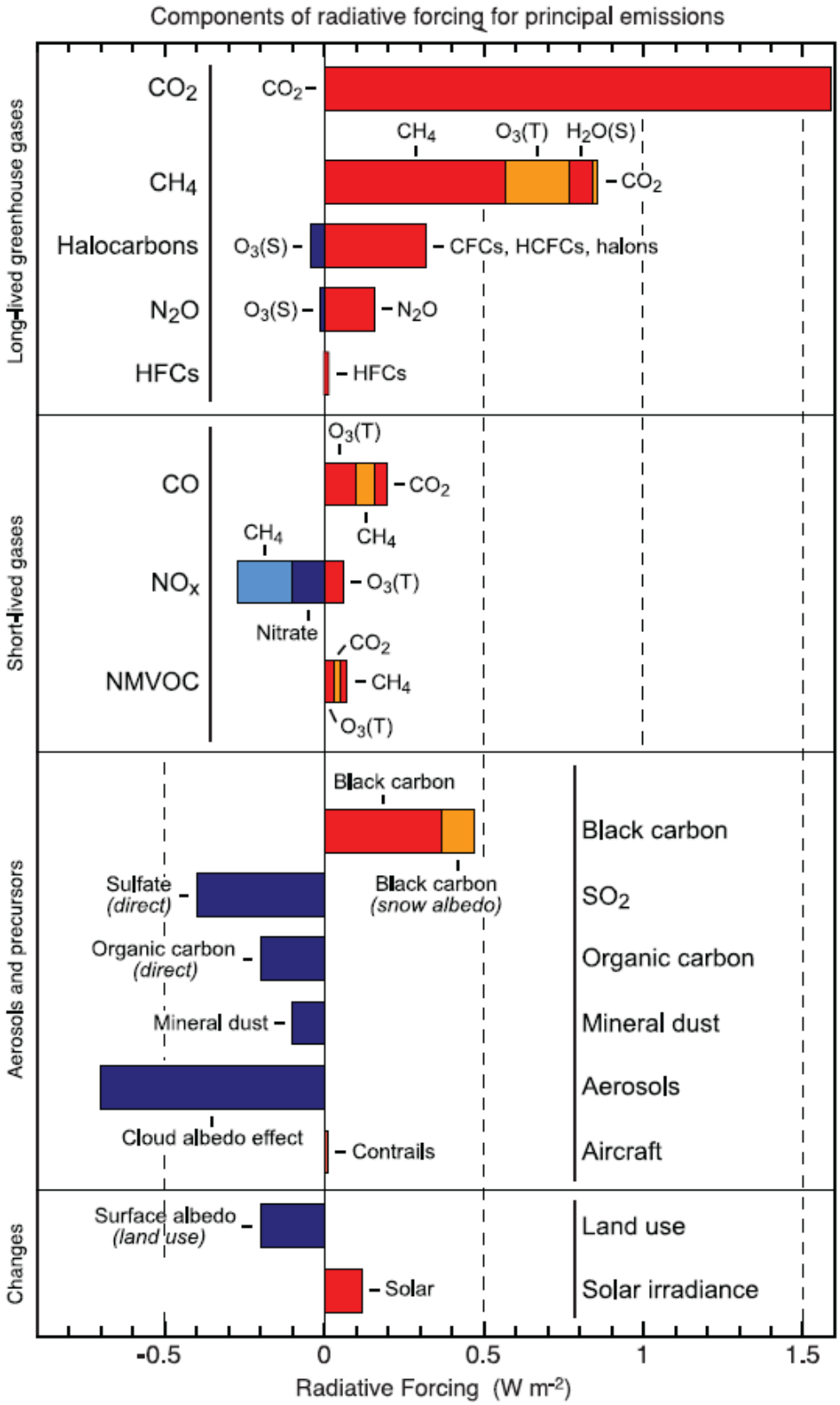

Figure 2.21. *Components of RF for emissions of principal gases, aerosols and aerosol precursors and other changes. Values represent RF in 2005 due to emissions and changes since 1750. (S) and (T) next to gas species represent stratospheric and tropospheric changes, respectively. The uncertainties are given in the footnotes to Table 2.13. Quantitative values are displayed in Table 2.13.*

Example of errors in unsuspected place: Weaver et al. (JAS,2002) calculating dust RF.

Model calculation for a dust over West Africa in summer 1988. Two optical properties of dust absorption are tested: strongly absorbing (pat), no absorbing (ili) in the visible.

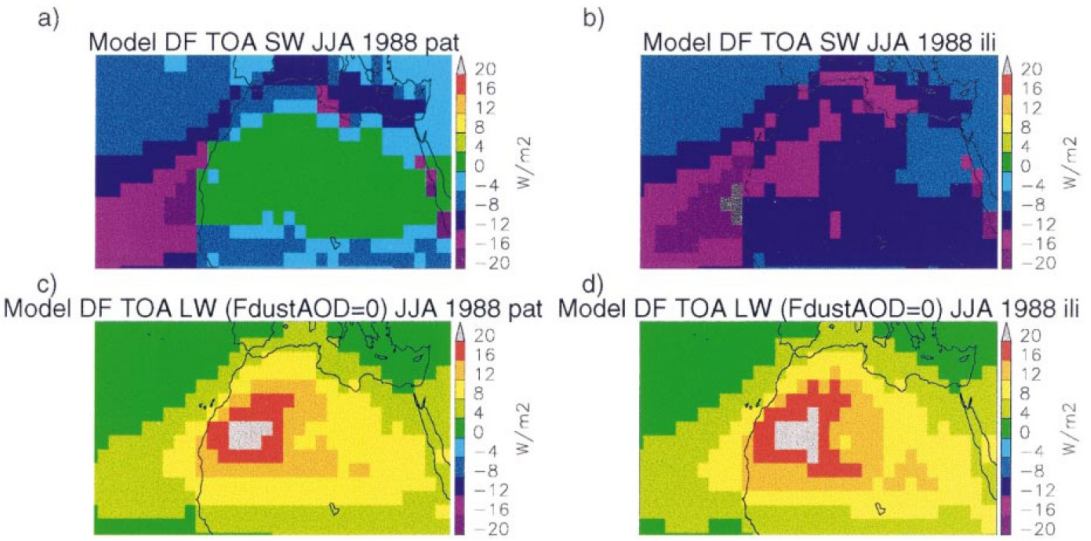

FIG. 7. Average Jun, Jul, and Aug 1988 daily TOA shortwave forcing using (a) Patterson and (b) illite optical parameters. Longwave forcing $\Delta F\downarrow = F_{dust}\downarrow - F_{dust}\downarrow$ (AOD = 0) using (c) Patterson and (d) illite optical parameters. Positive $\Delta F\downarrow$ values describe increased incoming or decreased outgoing radiation.

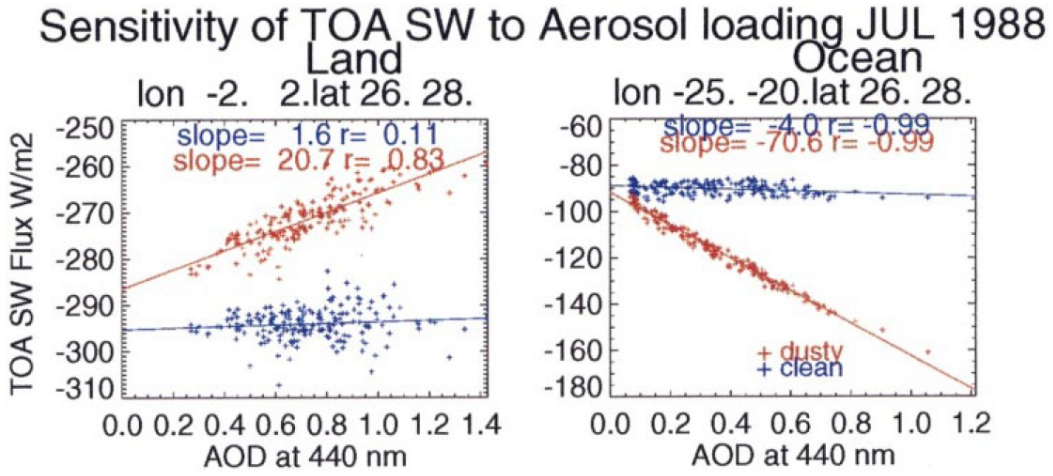

FIG. 3. Regression of outgoing TOA SW flux calculations against AOD in GOCART model during Jul 1988. On any given day each grid point will have a vertical profile of dust from the GOCART model, a shortwave flux, F_{dust} calculated using this profile and a flux that assumes a clean atmosphere F_{clean}. Both fluxes are plotted against the AOD from the GOCART profile using a red point for F_{dust} and a blue point for F_{clean}. Shown are regressions within a single 2° latitude by 5° longitude geographic box over land (left panel) and a single geographic box over ocean (right panel). The Patterson OP is used. Our sign convention has outgoing fluxes as negative.

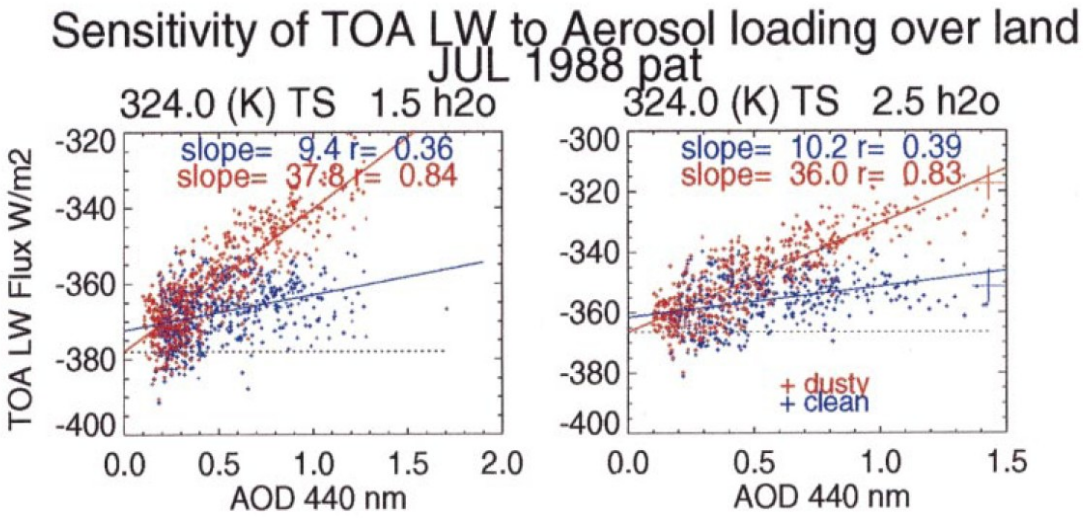

FIG. 5. Regression of outgoing TOA LW flux calculations against AOD in GOCART model during Jul 1988. On any given day each grid point will have a vertical profile of dust from the GOCART model, a longwave flux F_{dust} calculated using this profile and a flux that assumes a clean atmosphere F_{clean}. Both fluxes are plotted against the AOD from the GOCART profile using a red point for F_{dust} and a blue point for F_{clean}. Shown are regressions for grid locations over land with a surface temperature between 322.5 and 325.5 (K) during Jul 1988. The left panel has points with column water between 1.0 and 2.0 cm (very dry), the right panel has points between 2.0 and 3.0 cm (dry). Radiative calculations assume the Patterson OP. Our radiation sign convention has outgoing fluxes as negative.

Clearing dust contamination from TOVS retrieval of air temperature (Weaver et al., JGR, 2003)

HIRS-TOVS weighting functions for channels 8 (11.1 μm), 10 (12.56 μm), 11 (7.3 μm), 12 (6.7 μm).

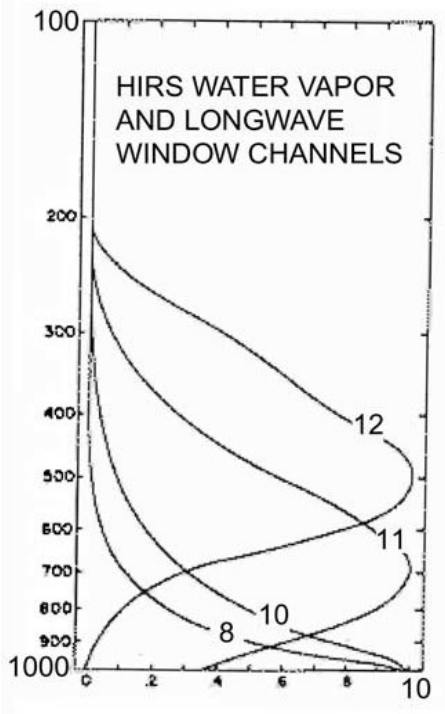

Difference of temperature at 800 hPa between TOVS retrieval from channel 8 and observations from NOAA as a function of dust concentration: There should be NO negative dependency of air temperature with dust!

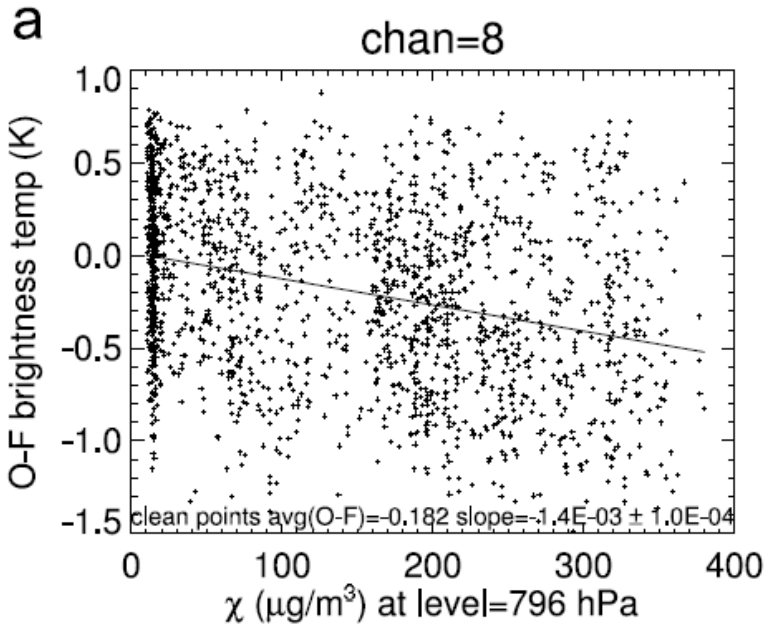

Correcting retrieved temperature to eliminate bias due to dust: case of August 15 1988 06Z

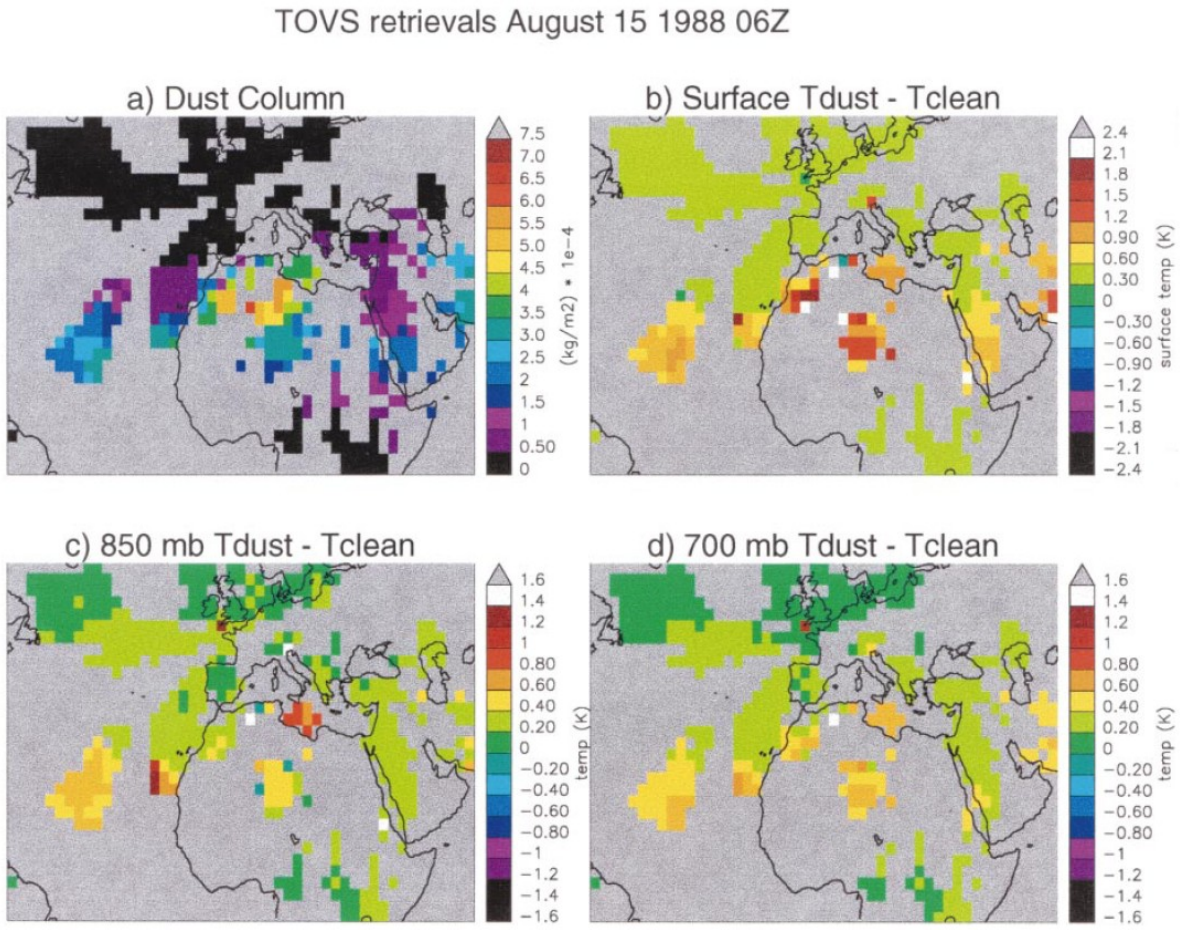

FIG. 11. Differences in temperatures from two types of retrievals on 15 Aug 1988. One retrieval, T_{dust}, assumes dust concentrations simulated from the GOCART model. (a) The GOCART simulated aerosol column loading. The second retrieval, T_{clean} assumes no dust. Retrievals are from simulated TOVS radiances that assume the GOCART dust concentrations. (b) $T_{dust} - T_{clean}$ at earth's surface, (c) at 850 mb and (d) at 700 mb.

The net DRE after dust clearing of temperature retrievals (Fclean) is lower than without clearing (FdustAOD=0) for both choice of optical properties: strong absorption with Patterson (pat) or weak absorption with illite (ili).

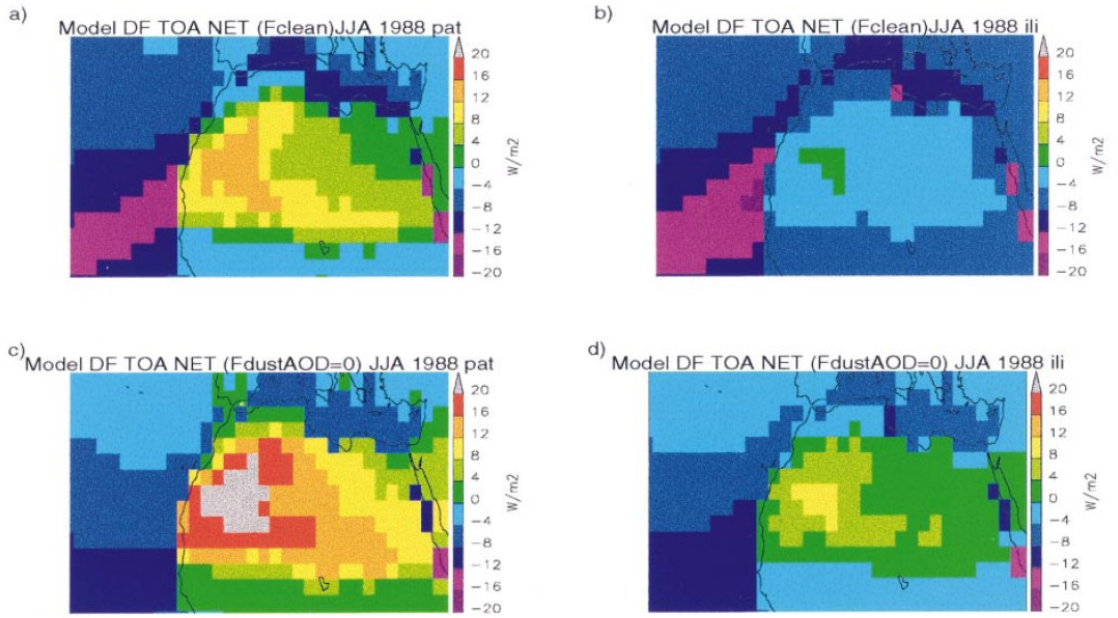

FIG. 8. Average Jun, Jul, and Aug 1988 net TOA forcing. Calculation where LW uses $\Delta F\downarrow = F_{\text{dust}}\downarrow - F_{\text{clean}}\downarrow$ using (a) Patterson and (b) illite optical parameters. Calculation where LW uses $\Delta F\downarrow = F_{\text{dust}}\downarrow - F_{\text{dust}}\downarrow$ (AOD = 0) using (c) Patterson and (d) illite optical parameters. Positive $\Delta F\downarrow$ values describe increased incoming or decreased outgoing radiation.